

# A study of $\text{Nd}_2\text{Fe}_{14}\text{B}$ and a neodymium-rich phase in sintered NdFeB magnets

J. HOLC, S. BESENIČAR, D. KOLAR

*J. Stefan Institute, E. Kardelj, University, Ljubljana, Yugoslavia*

The microstructure and properties of NdFeB sintered permanent magnets were analysed by different methods. Samples analysed were sintered and thermally treated. The hard magnetic  $\text{Nd}_2\text{Fe}_{14}\text{B}$  phase and amorphous neodymium-rich phase were observed by TEM. The neodymium-rich phase contained iron and boron, in elemental and in  $\text{B}_2\text{O}_3$  form, which is known as a glass former. At the sintering temperature,  $\text{Nd}_2\text{Fe}_{14}\text{B}$  and the neodymium-rich phase are supersaturated with iron, which should be dissolved at the annealing temperature to react with neodymium and boron and form additional  $\text{Nd}_2\text{Fe}_{14}\text{B}$  phase. Iron precipitates of size up to 2 nm were detected in the  $\text{Nd}_2\text{Fe}_{14}\text{B}$  phase. These superparamagnetic precipitates of  $\alpha$ -Fe could affect the hard magnetic properties of NdFeB magnets.

## 1. Introduction

Sintered Fe-Nd-B magnetic alloys based on the compound  $\text{Nd}_2\text{Fe}_{14}\text{B}$  have attracted the attention of many researchers as a material for use as a new type of permanent magnet [1]. The highest energy product of such sintered magnets was attained with the composition  $\text{Nd}_{15}\text{Fe}_{77}\text{B}_8$  [1], which contains an excess of neodymium and boron as compared with the pure magnetic phase  $\text{Nd}_2\text{Fe}_{14}\text{B}$ .

In principle three types of phases have been identified in the sintered magnets [2-4]: a hard magnetic phase,  $\text{Nd}_2\text{Fe}_{14}\text{B}$ , with a tetragonal crystal structure as the major phase; a soft magnetic phase which is boron rich with the composition  $\text{Nd}_{1+x}\text{Fe}_4\text{B}_4$ , and a neodymium-rich liquid phase sintering aid. Additional phases visible in the microstructure are  $\text{Nd}_2\text{O}_3$ , in some cases iron and iron-rich phase precipitates, and an "exotic" phase [5].

Recently the role of oxygen contamination has received attention. Oxygen contamination phases have been found at the grain boundaries and grain junctions of these magnets [6].

The aim of our work was to clarify the appearance of the different magnetic and non-magnetic phases in the microstructure of NdFeB magnets as a function of the preparation parameters.

## 2. Experimental

The raw material was commercially available NdFeB powder (Th. Goldschmidt AG., FRG) with the composition 30.6 wt % Nd, 3.1 wt % Dy, 64 wt % Fe, 1.2 wt % B and an oxygen content of 0.3 wt %.

The coarse powder was ball milled in *n*-hexane in a stainless steel container with stainless steel balls. The powder was aligned in a pulsed magnetic field of approximately 5 T and isostatically pressed with a pressure of 700 MPa. Samples were sintered in a vacuum furnace at a pressure of  $10^{-3}$  Pa and a temperature of 1080°C for 1 h. The sintered samples

were cooled rapidly. Post sintering treatments were performed at 600 to 650°C *in vacuo*, or in a helium atmosphere for 1 h and then quenched.

The final oxygen content of the sintered NdFeB samples was 0.5 to 0.7 wt % (Ströhlein Oxygen Analyser).

After the sintering process, the samples were magnetized and characterized by magnetic properties measurements.

The specimens for TEM were prepared by grinding and subsequent argon atom milling (Ion Tech). Thin foils were examined in a JEOL JEM 2000 FX transmission electron microscope. Samples for Auger electron spectroscopy were mechanically polished and positioned in the vacuum chamber of a PHI SAM 545 Auger spectrometer. The samples were ion etched prior to analysis.

The microstructures of the samples were analysed on polished surfaces by optical and SEM microscopy.

DTA analysis of NdFeB samples was done with Netzsch STA 429 equipment in a vacuum at  $10^{-3}$  Pa. The heating rate was  $10^\circ\text{C min}^{-1}$  and the final temperature 900°C.

## 4. Results and discussion

### 4.1. Hard magnetic phase

Microstructure analysis of as-sintered and as-sintered and annealed samples showed crystalline hard magnetic phase  $\text{Nd}_2\text{Fe}_{14}\text{B}$  (T1) and an amorphous phase. TEM analysis showed several characteristic features.

Fig. 1 shows a transition area between the hard magnetic phase and the amorphous phase. The transition between the amorphous phase (in the right-hand corner of the picture) and the remaining crystallized area is continuous. The relevant selected area diffraction patterns are presented in Figs 2a and 2b. The diffraction pattern of the amorphous regions (Fig. 1a) shows only a broad diffraction ring with a mean value of  $d = 0.3$  nm. From the diffraction

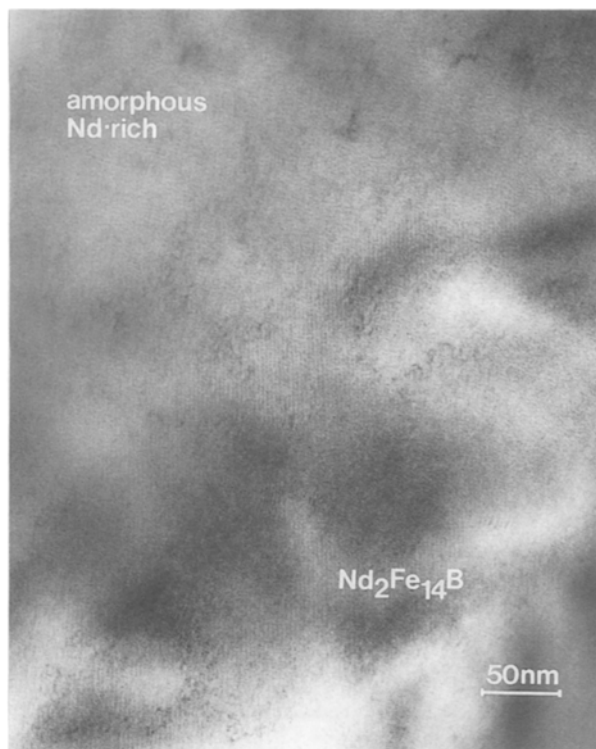


Figure 1 Transmission electron micrograph of the transition between  $\text{Nd}_2\text{Fe}_{14}\text{B}$  and the amorphous phase in a NdFeB sample (sintered at  $1080^\circ\text{C}$  for 1 h, annealed at  $620^\circ\text{C}$  for 1 h and quenched in helium atmosphere).

patterns of the T1 phase (Fig. 1b)  $[001]$  zone axis in the sintered sample is evident that reflections of type (140) and (330) are stronger, and correspond to values of intensities which were obtained by X-ray diffraction on a  $\text{Nd}_2\text{Fe}_{14}\text{B}$  [10].

In the sintered and annealed samples, besides T1 phase, we also identified the diffraction patterns of microcrystalline  $\alpha\text{-Fe}$  (Fig. 3). In the dark field image

TABLE I Changes in some properties of NdFeB magnets after thermal treatment at  $620^\circ\text{C}$  for 1 h *in vacuo*

| Sample          | Density ( $\text{g cm}^{-3}$ ) | T1 phase (%) | $B_r$ (mT) |
|-----------------|--------------------------------|--------------|------------|
| As-sintered (A) | 7.48                           | 87           | 1190       |
| Annealed (B)    | 7.50                           | 92           | 1220       |

(Fig. 3) of the T1 phase, taken with the (011) reflection of the  $\alpha\text{-Fe}$  phase the precipitates are bright. The relevant diffraction pattern is presented in Fig. 4. It is known that the hard magnetic  $\text{Nd}_2\text{Fe}_{14}\text{B}$  phase exists over a range of composition [9, 19]. On quenching or quick cooling, excess iron precipitates as  $\alpha\text{-Fe}$  crystallites within the grains of T1 phase.

$\alpha\text{-Fe}$  precipitates in sintered NdFeB magnets have already been noticed [9, 10]. In disagreement with the observations of other authors [21], the magnitude of the  $\alpha\text{-Fe}$  precipitates in our samples was only up to 2 nm (Fig. 4). Tentative explanation of the deformation of diffraction spots on (011) reflections could be the consequence of stressed  $\alpha\text{-Fe}$  precipitates in the unchanged T1 matrix phase. This could be also the reason for the inhibited growth of the precipitates.

We noticed that the sintered densities increased, when the samples were subjected to a thermal treatment procedure at 600 to  $650^\circ\text{C}$ ; the density of T1 is the highest of all the phases present. On the other hand, by quantitative analysis of the microstructures of both samples (A and B) we confirmed a higher content of T1 phase in annealed (B) samples. In addition, a systematic increase of remanent magnetization was noticed in these samples. All these property changes are summarized in Table I.

Under a slow cooling rate and annealing treatment, the excess iron reacts with the neodymium-rich phase. Therefore the additional T1 phase is formed on the

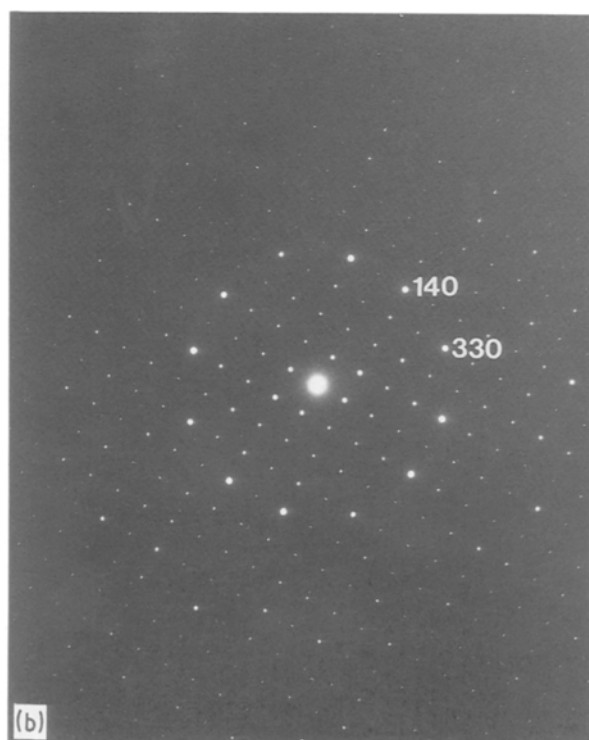
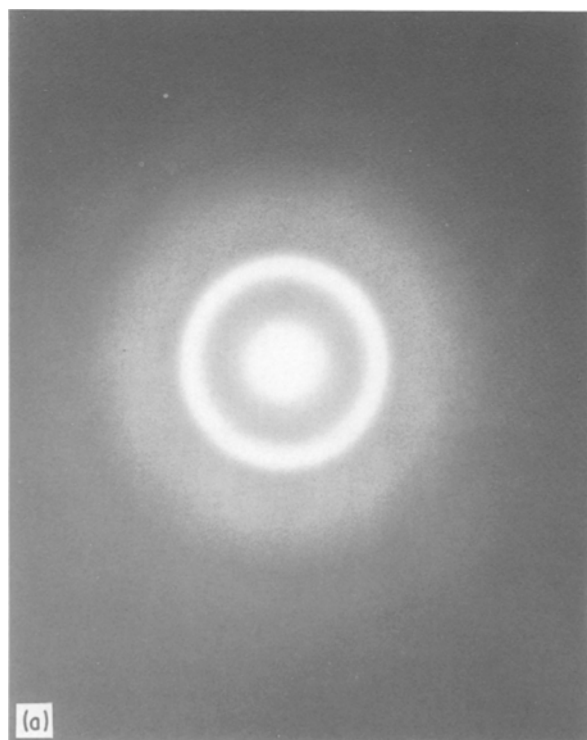


Figure 2 Electron diffraction pattern of (a) amorphous phase and (b)  $\text{Nd}_2\text{Fe}_{14}\text{B}$  phase, zone axis  $[001]$ .

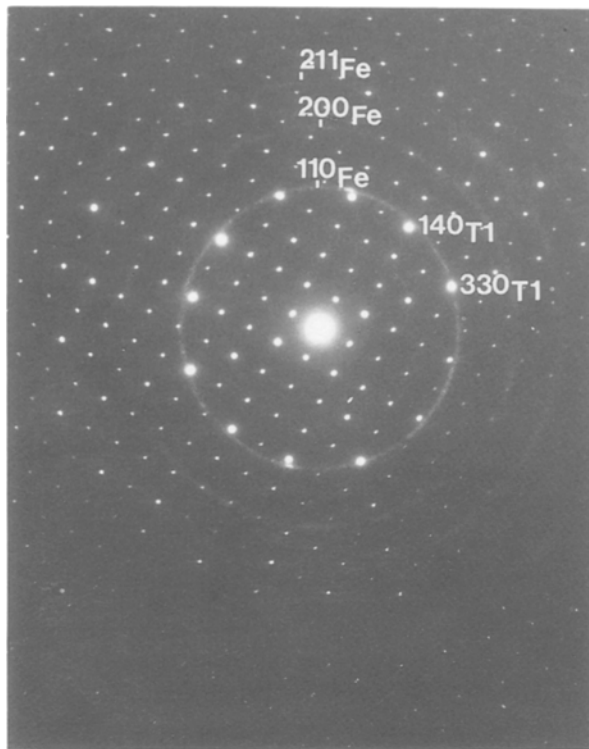


Figure 3 Electron diffraction pattern of NdFeB sample, sintered at 1080° C for 1 h, quenched *in vacuo*: Nd<sub>2</sub>Fe<sub>14</sub>B phase zone axis [001] and  $\alpha$ -Fe.

grain boundaries from neodymium, iron and boron which are present in the neodymium-rich phase, and thus the quantity of neodymium-rich phase is minimized. There are also some data in the literature about the precipitation of T1 phase on the grain boundaries [14]; this precipitation might be one of the main reasons for the diminution of crystal damage due to the milling process.

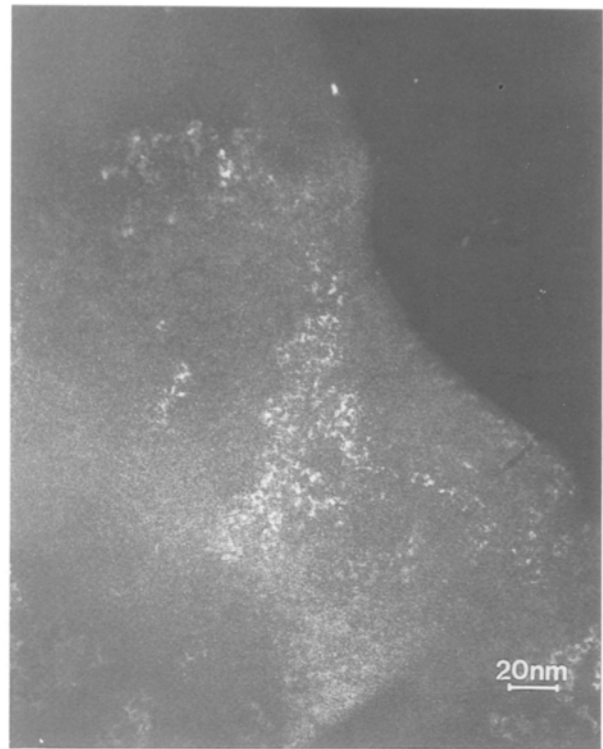


Figure 4 Dark field image of  $\alpha$ -Fe precipitates in Nd<sub>2</sub>Fe<sub>14</sub>B phase.

#### 4.2. Amorphous neodymium-rich phase

The neodymium-rich phase in sintered NdFeB magnets is rather complex and its structure and significance is still not completely understood. The phase is neodymium-rich as compared with the T1 grains; however, its structure was identified by some authors as a bcc type structure [7] a dhcp structure [13] or as an fcc structure [6], respectively. It was established that this neodymium-rich phase could be present in an

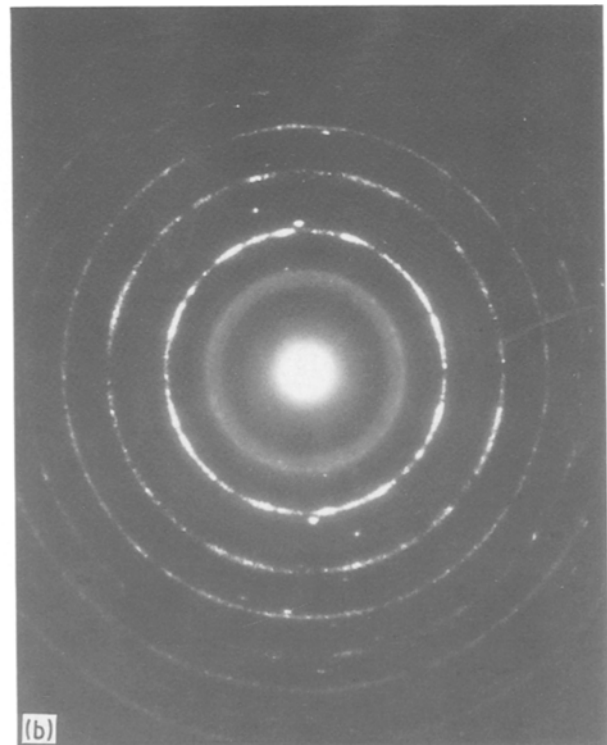


Figure 5 (a) Transmission electron micrograph of  $\alpha$ -Fe precipitates in amorphous phase in a sample sintered at 1080° C for 1 h and quenched in helium atmosphere.

amorphous state [7, 12] and also that oxygen might be present [6]. The latest microstructure investigations showed that the neodymium-rich phase could have a different neodymium to iron ratio [9]. Our analysis confirms the view that the neodymium-rich phase is amorphous.

Conflicting literature data and our observations can be explained by assuming that the neodymium-rich phase is saturated with iron at the sintering temperature. At a rapid cooling rate this phase remains unstable in sintered and quenched samples, however electron bombardment in an electron microscope induces crystallization of excess  $\alpha$ -Fe (bcc phase). Fig. 5a shows such a region, together with the diffraction pattern (Fig. 5b). Besides the broad diffraction ring of the amorphous phase, the diffraction pattern of microcrystalline  $\alpha$ -Fe precipitates can also be identified. The same effect may be achieved by ion erosion and this may explain the finding of a bcc structure by those authors who used ion erosion for preparation of the samples [6, 7, 10, 12]. In contrast, those authors who used electropolishing [6, 9, 11] established that the structure is of dhcp [9] or fcc type [6]. It could be expected that electropolishing in a mixture of ethanol and perchloric acid would cause oxidation of neodymium to neodymium oxides because of its high susceptibility to oxidation. Further, boron may be extracted from the neodymium-rich phase because of the solubility of  $B_2O_3$  in ethanol.

The presence of the oxide inclusions such as  $Nd_2O_3$  or  $B_2O_3$  was confirmed by Auger electron spectroscopy as demonstrated on an oxygen map (Fig. 6).

The presence of  $B_2O_3$  was also indicated by differential thermal analysis. For both samples (sintered, and sintered plus annealed) the broad peak in the temperature range from 410 to 500°C could be attributed to  $B_2O_3$  melting ( $T_m = 460^\circ C$ ), because of the glassy structure of boron oxide. The other peaks between 630 and 750°C could be the consequence of melting of the neodymium-rich phase [14–16]. The presence of oxygen in the neodymium-rich phase and reactions in the neodymium-rich phase could be responsible for the non-reproducibility of DTA peaks of the neodymium-rich phase. This was established previously by phase equilibria investigations in the Nd–Fe–B system [20].

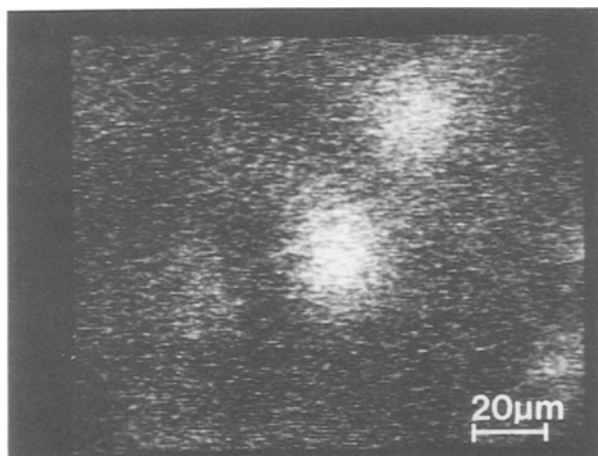


Figure 6 Auger electron map of oxygen in the NdFeB sample.

$B_2O_3$  is well known as a compound which forms a glassy phase and that is probably the reason why the amorphous neodymium-rich phase remains in this state during cooling. Stadelmaier [17] was the first to propose that  $B_2O_3$  and neodymium and iron forms metastable glassy phase.

We presume that  $B_2O_3$  arose as a reaction product from the oxidized surface of the matrix alloy containing boron at elevated temperature. It is well known that the rare earth oxides react with boron and form rare earth borides and boron oxide [18]. Hence, we propose that this reaction “cleans” the T1 grains in such a way that  $Nd_2O_3$  reacts with the boron. Otherwise  $Nd_2O_3$ , because of its high melting point, could form a barrier between T1 grains and thus hinder the sintering process.

The decisive importance of  $B_2O_3$  as a slag former and a sintering acceleration agent has already been mentioned [17].

Usually the oxygen content in sintered magnets is from 0.2 to 0.8 wt %. This should also be the upper limit for good magnetic properties, and this was also confirmed in our investigations. Most microstructural investigations, including ours, showed a relatively small content of  $Nd_2O_3$  inclusions, which confirms the presumption that the oxygen is mainly present elsewhere.

#### 4.3. Influence of inclusions on magnetic properties

$\alpha$ -Fe precipitates in the T1 phase might act as pinning centres for magnetic domain walls, provided that they are small enough to be superparamagnetic [22]. The presence of small  $\alpha$ -Fe precipitates may explain the difference in the magnetic properties of samples annealed at 620°C and those quenched in a helium atmosphere or *in vacuo*. Fig. 7 shows demagnetization curves of both samples, where a characteristic kink in the curve of the helium cooled sample may be noticed. We believe that rapid cooling due to the high thermal conductivity of helium suppresses the precipitation of

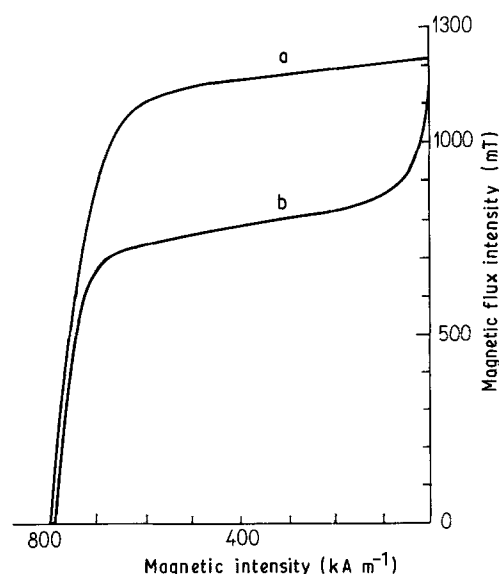


Figure 7 Demagnetization curves for samples: (a) sintering at 1080°C, annealing at 620°C and quenching *in vacuo*. (b) Sintering at 1080°C, annealing at 620°C and quenching in helium atmosphere.

$\alpha$ -Fe precipitates in the T1 phase. On the other hand, slower cooling in a vacuum favours precipitation, although the final size must not exceed the value where detrimental soft magnetic behaviour prevails.

## 5. Conclusions

Microstructural investigation of NdFeB magnets revealed several possible reasons for the improvement of hard magnetic properties during an appropriate heat treatment. An important feature seems to be the increased solubility of iron in the hard magnetic phase at high temperatures. During the annealing process, the quantity of hard magnetic phases increases due to reaction of excess iron with the neodymium-rich phase.

On the other hand, precipitation of  $\alpha$ -Fe on fast cooling could contribute to magnetic hardening.

The neodymium-rich phase accumulates most of the oxygen impurities. The amorphous nature of neodymium-rich phase may be due to formation of  $B_2O_3$ .

## Acknowledgements

This work was financially supported by the Research Council of SR Slovenia. The authors would like to thank Dr V. Kraševc for electron microscope analysis and stimulating discussion.

## References

1. M. SAGAWA, S. FUJIMURA, M. TAGAWA and Y. MATSUURA, *J. Appl. Phys.* **55** (1984) 2083.
2. J. FIDLER and L. YANG, Proceedings of the 4th International Symposium on Magn. Anisotropy and Coercivity in Rare-Earth-Transition Metal Alloys, Dayton, 1985, edited by K. J. Strnat, University of Dayton, p. 647.
3. M. SAGAWA, S. FUJIMURA, H. YAMAMOTO, Y. MATSUURA, S. HIROSAWA and K. HIRAGA, Proceedings of the 4th International Symposium on Magn. Anisotropy and Coercivity in Rare-Earth-Transition Metal Alloys, Dayton, 1985, edited by K. J. Strnat, University of Dayton, p. 587.
4. K. H. BUSCHOW, D. B. DE MOOIJ, J. L. C. DAAMS and H. M. VAN NOORT, *J. Less Common Met.* **115** (1986) 357.
5. J. FIDLER, Proceedings of the 5th International Symposium on Magn. Anisotropy and Coercivity in Rare-Earth-Transition Metal Alloys, Bad Soden, FRG, 1987, edited by Deutsche Physikalische Gesellschaft, Bad Honnef, p. 363.
6. R. REMESH, J. K. CHEN and G. THOMAS, *J. Appl. Phys.* **61** (1987) 2993.
7. K. HIRAGA, M. HIRABAYASHI, M. SAGAWA and Y. MATSUURA, *Jpn J. Appl. Phys.* **24** (1985) 699.
8. H. BOLLER and H. OESTEREICHER, *J. Less Common Met.* **103** (1984) L5.
9. J. FIDLER, Proceedings of the 5th International Symposium on Magn. Anisotropy and Coercivity in Rare-Earth-Transition Metal Alloys, Bad Soden, FRG, 1987, edited by Deutsche Physikalische Gesellschaft, Bad Honnef, p. 363.
10. X. HONGZU, L. SHOHYI, Y. MEIJUAN and G. BINGLIN, *ibid.* p. 411.
11. P. SHUMING, Z. ZHIPO and M. RUZHANG, *ibid.* p. 305.
12. M. SAGAWA, S. HIROSAWA, Y. TSUBOKAWA and R. SHIMZU, *ibid.* p. 229.
13. J. FIDLER, *IEEE Trans. Mag.* **MAG-21** (1985) 1955.
14. H. H. STADELMAIER, N. A. EL-MASRY, N. C. LIU and S. F. CHENG, *Mater. Sci. Lett.* **2** (1984) 411.
15. Y. MATSUURA, S. HIROSAWA, H. YAMAMOTO, S. FUJIMURA, M. SAGAWA and K. OSAMURA, *Jpn J. Appl. Phys.* **24** (1985) L635.
16. G. SCHNEIDER, E. T. HENIG, H. H. STADELMAIER and G. PETZOW, Proceedings of the 5th International Symposium on Magn. Anisotropy and Coercivity in Rare-Earth-Transition Metal Alloys, Bad Soden, FRG, 1987, edited by Deutsche Physikalische Gesellschaft, Bad Honnef, p. 347.
17. H. H. STADELMAIER and N. A. EL-MASRY, Proceedings of the 4th International Symposium on Magn. Anisotropy and Coercivity in Rare-Earth-Transition Metal Alloys, Dayton, 1985, edited by K. J. Strnat, University of Dayton, p. 613.
18. G. BLIZNAKOV and P. PESHEV, *J. Less Common Met.* **7** (1964) 441.
19. K. H. J. BUSCHOW, D. B. DE MOOIJ, J. L. C. DAAMS and H. M. VAN NOORT, *ibid.* **115** (1986) 357.
20. T. S. CHIN, D. S. TSAI, Y. H. CHANG, S. E. HSU and M. P. HUNG, Proceedings of the 5th International Symposium on Magn. Anisotropy and Coercivity in Rare-Earth-Transition Metal Alloys, Bad Soden, FRG, 1987, edited by Deutsche Physikalische Gesellschaft, Bad Honnef, p. 403.
21. J. FIDLER and Y. TAWARA, *IEEE Trans. Magn.* **MAG-24** (1988) 1951.
22. M. MCCAIG, "Permanent Magnets in Theory and Practice" (Pentech Press, London, 1977) p. 47.

Received 16 September 1988  
and accepted 24 February 1989